Colloids and Surfaces B: Biointerfaces 228 (2023) 113433

Contents lists available at ScienceDirect

Colloids and Surfaces B: Biointerfaces

journal homepage: www.elsevier.com/locate/colsurfb

Contrasting transport and fate of hydrophilic and hydrophobic bacteria in wettable and water-repellent porous media: Straining or attachment?

Nasrollah Sepehrnia [a,*], Mohsen Gorakifard [b], Paul D. Hallett [a], Mohammad Ali Hajabbasi [c], Nima Shokri [d], Mark Coyne [e]

[a] School of Biological Sciences, University of Aberdeen, Aberdeen, UK
[b] Department of Mechanical Engineering, Universitat Rovira i Virgili, Spain
[c] Department of Soil Science, College of Agriculture, Isfahan University of Technology, Isfahan 84156-83111, Islamic Republic of Iran
[d] Institute of Geo-Hydroinformatics, Hamburg University of Technology, Am Schwarzenberg-Campus 3 (E), 21073 Hamburg, Germany
[e] University of Kentucky, Department of Plant and Soil Sciences, United States

ARTICLE INFO

Keywords:
Interfacial processes
Wetting characteristics
Pore-scale processes
Vadose zone
Drought

ABSTRACT

Bacterial transport and retention likely depend on bacterial and soil surface properties, especially hydrophobicity. We used a controlled experimental setup to explore hydrophilic *Escherichia coli* (*E. coli*) and hydrophobic *Rhodococcus erythropolis* (PTCC1767) (*R. erythropolis*) transport through dry (− 15,000 cm water potential) and water saturated (0 cm water potential) wettable and water-repellent sand columns. A pulse of bacteria (1×10^8 CFU mL^{-1}) and bromide (10 mmol L^{-1}) moved through the columns under saturated flow (0 cm) for four pore volumes. A second bacteria and bromide pulse was then poured on the column surfaces and leaching was extended six more pore volumes. In dry wettable sand attachment dominated *E. coli* retention, whereas *R. erythropolis* was dominated by straining. Once wetted, the dominant retention mechanisms flipped between these bacteria. Attachment by either bacteria decreased markedly in water-repellent sand, so straining was the main retention mechanism. We explain this from capillary potential energy, which enhanced straining under the formation of water films at very early times (i.e., imbibing) and film thinning at much later times (i.e., draining). The interaction between the hydrophobicity of bacteria and soil on transport, retention and release mechanisms needs greater consideration in predictions.

1. Introduction

The widespread contamination of soils and groundwater by microbes can deteriorate their quality and threaten human and environmental health [1–8]. Microbes may also be introduced to soils and groundwater to remove recalcitrant pollutants (i.e., hyper-hydrophobic petroleum components) through bioaugmentation techniques [6]. Bacterial contamination or bioaugmentation efficacy depend on bacteria transport, but this is difficult to predict because of the complex interactions between bacteria and soil mineral surfaces that vary depending upon environmental conditions [1–10].

A primary dynamic property controlling the transport and retention of bacteria is soil water content, with bacteria retention generally increasing with decreasing water content [7–10]. Physicochemical (i.e., attachment and detachment) and physical (i.e., straining) mechanisms that control bacteria transport and retention in porous media have been described in ideal laboratory conditions [3–10]. However, these tests under steady state conditions do not reflect transport that may occur in the field during a rainfall event. When moving from the soil surface, downwards, bacteria may experience a drier passage from upper to lower zones to reach the deeper layers, such as groundwater in soils. This variability of soil moisture with depth adds complexity to bacteria fate due to immobile water zones, film straining, attachment to air–water interfaces, and air–water–solid contact lines [6]. As soil moisture is related to precipitation and temperature, climate change could exacerbate drier surface soils [11–14].

By extension, as soils dry, their wettability (or hydrophobicity) can change [11,14]. For hydrophilic soils, greater retention of bacteria as soil dries has been attributed to enhanced stagnant regions within the pore structure under unfavorable attachment conditions [11]. Most soils are not entirely hydrophilic, resulting in heterogeneous wetting patterns in time and space that produce preferential flow paths that may hasten

* Corresponding author.
E-mail address: nasrollah.sepehrnia@abdn.ac.uk (N. Sepehrnia).

https://doi.org/10.1016/j.colsurfb.2023.113433
Received 2 February 2023; Received in revised form 12 June 2023; Accepted 27 June 2023
Available online 28 June 2023

microbial and colloidal transport [11–14]. Particle surface wettability can govern the spatial heterogeneity of water flow and retention [15–17]. This behavior of soil has prompted considerable research exploring solute transport by preferential and finger flows (e.g., [18]), but an extension of such research to bacteria and colloids transport is lacking [11,12].

In one of the few available studies, Sepehrnia et al. [11] found enhanced bacteria retention for the rewetting of initially dry wettable soil, but more release and transport of bacteria if the soil was naturally hydrophobic. Moreover, this study also found that bacteria surface properties had a large effect, with hydrophobic *R. erythropolis* having enhanced release and transport compared to hydrophilic *E. coli*. In previous studies, bacteria hydrophobicity/hydrophilicity effects were masked by porous media and water flow characteristics [19,20].

There are several characteristics of porous media and microbial cells that affect bacterial transport, retention, and release by straining and attachment. Cell size is a major driver as it affects straining [19], which interacts with porous media particle size. One study found that coarse media (i.e., sand 0.58–1.48 mm) had similar retention of hydrophobic and hydrophilic bacteria, so it was not possible to discriminate the predominant mechanism of bacteria retention [20]. For fine sand media (e.g., 0.25–0.54 mm) in the same study, however, hydrophilic bacteria straining (i.e., *E. coli* and *Klebsiella sp.*) was dominated by straining, but attachment had the same importance as straining for hydrophobic bacteria (i.e., *R. rhodochrous*) [20]. Thus, the relative implication of cell properties remains unclear [11,12,19,20].

The importance of the governing mechanisms in bacteria fate and transport under extremely dry conditions of wettable and water-repellent soils are also poorly understood [11,12]. This is perhaps due to the complexity of the physical, chemical, and biological interactions between bacteria cell properties [19–21] and soils in dry conditions, making it a grand challenge to understand the fundamentals governing these processes [6,11,12].

Evidence suggests that bacterial hydrophobicity interacts with soil wettability to affect transport properties through attachment and straining of bacteria and wetting front development of infiltrating water. Using leaching experiments in the laboratory, we explored infiltration and leaching from dry (− 15,000 cm water potential) to very close to saturation conditions (0 cm water potential) of soil [11,12]. The main objective of this research was to distinguish between the governing transport and retention mechanisms of contrasting hydrophilic *E. coli* and hydrophobic *R. erythropolis* (PTCC1767) through wettable and hydrophobic porous media in dry and wetted states imposed by a continuous saturated flow condition. We specifically discuss findings in terms of attachment and straining of bacteria, including the contribution of film straining in bacteria retention. The breakthrough curves (BTCs) of bacteria were modeled using the modified form of the advection-dispersion equation (the Two Kinetics Sites model) considering non-equilibrium chemical conditions, which are used for microbial transport and retention [6].

2. Material and methods

2.1. Preparation of sand columns and bacteria suspensions

Sand columns were prepared according to Bolster et al. [22] and Sepehrnia et al. [12] with washed and dried (at 105 °C) wettable sand materials (63.4 % fine < 0.25 mm, 36.3 % medium, and 0.3 % coarse > 0.5 mm). The wettability of sand particles was changed by polygalacturonic acid (PGA), which created wettable (contact angle, CA: 0°) and water-repellent (CA: 92° ± 4.1°) surfaces [8]. The CA was measured using the sessile drop method (see [11,14]). The wettable and water-repellent sands were air-dried and separately packed into columns of 18.2 cm height and 7 cm diameter at 1.53 g cm^{-3} bulk density and porosity equal to 0.42. The sand had a particle density of 2.65 g cm^{-3}.

The details of bacteria properties are described in Sepehrnia et al. [11,12] and we thus briefly summarize the information. *E. coli* (approx. 2.05 μm in length and 1.2 μm in width) and *R. erythropolis* (PTCC1767) (approx. 1.47 μm in length and 1.1 μm in width) were grown on solid Nutrient Agar for 24 and 48 h, respectively. The growth was removed using deionized distilled water and suspended in a solution containing 10 mM Br^- to prepare 1.00×10^8 CFU mL^{-1} concentration based on optical density (OD) with a UV–vis spectrophotometer (Jenway, 6505) at 518 nm for *E. coli* and 509 nm for *R. erythropolis*. Microbial adhesion to ultra-hydrophobic hydrocarbon testing surfaces (MATH) showed the bacteria cell hydrophobicity was 11 % for *E. coli* and 73 % for *R. erythropolis* [12].

2.2. Leaching process

Hydrophilic *E. coli* or hydrophobic *R. erythropolis* (PTCC1767) and bromide (Br^-, KBr), as a chemical tracer, were simultaneously infiltrated into the columns as the influent. The bacteria concentrations were 1.0×10^8 CFU mL^{-1} and Br^- concentration was 10 mmol L^{-1}. Leaching was performed over two pulses. First, 62 mL of the influent was poured on the top of the air-dried wettable and water-repellent sand columns. Then, a saturated flow condition was applied to leach the dry columns by a disc infiltrometer [11,12]. Leaching of the sand columns continued for four pore volumes (PVs) referred to as Pulse I (dry infiltration). For the second pulse, referred to as Pulse II (wet infiltration) the influent was subsequently poured on the surface of the columns and leached for a further 6 PVs. *Escherichia coli* and *R. erythropolis* bacteria transport was studied in separate columns to avoid interactions between the bacteria and to simplify quantification of bacteria transport. The influent solution was prepared a few minutes before the leaching experiment, and the injection was done shortly for either pulse [11,12], therefore, death and growth of bacteria in the influent and the columns as well as the effluents was minimized.

2.3. Monitoring of bacteria concentrations

Bacteria concentrations in the effluents were monitored at 0.1 pore volume intervals for the first pore volume and at 0.25 pore volumes for the next three pore volumes, respectively. After leaching, the deposition patterns of bacteria in the sand matrices were assessed by segmenting the columns into six 3-cm layers in three replicates at each depth (data are not shown). To dilute effluents, one gram of sand was poured into 9 mL deionized sterile water and agitated, then shaken using a vortex mixer (VWR International, Germany) at 300 rpm to release bacteria from the sand surface. The plate-count method was used to enumerate *E. coli* and *R. erythropolis* cultured on Eosin Methylene Blue and Nutrient Agar medium cultures, respectively [12]. Bacteria colonies were counted as colony forming units per milliliter (CFU mL^{-1}) and dry weight (CFU g^{-1}) after 24 h for *E. coli* and 48 h for *R. erythropolis*.

2.4. Modeling

Simulations of Br^- and bacteria transport were separately performed for dry and wet pulses. For Br^-, inverse optimizations were performed using the Mobile Immobile Model (MIM) with non-equilibrium physical condition for solute transport (see Šimůnek et al. [23]) implemented in HYDRUS-1D (version 4.16.0110) (PC Progress, Riverside, USA).

$$\theta_m \frac{\partial C_m}{\partial t} + \theta_{im} \frac{\partial C_{im}}{\partial t} = \theta_m D_m \left(\frac{\partial^2 C}{\partial x^2} \right) - \theta_m v_m \frac{\partial C_m}{\partial x} \quad (1)$$

$$\theta_{im} \frac{\partial C_{im}}{\partial t} = \alpha \left(C_m - C_{im} \right) \quad (2)$$

Where C is Br^- concentration in the soil solution [mL^{-3}], t is time [T], ν is pore water velocity [L T^{-1}], D is dispersion coefficient [L^2 T^{-1}] yielded from dispersivity (λ, [L^{-1}]) and apparent pore water velocity ($D = \lambda\nu$)

[LT^{-1}]. Subscripts $_m$ and $_{im}$ refer to mobile and immobile water regions.

The experimental data were optimized to simulate Br^- dispersivity (λ), saturated and immobile water contents (θ_s and θ_{im}), saturated hydraulic conductivity (K_s), and mass transfer coefficient for Br^- exchange between mobile and immobile liquid regions (α). Bromide was not excluded from the immobile regions due to the dynamics of sand wettability and the initial dry conditions of the columns and thus the exchange of Br^- between the mobile and immobile regions ($\alpha \ddagger 0$). Note that this aspect was simplified ($\alpha = 0$) in other studies (e.g., [21]).

The predicted hydraulic characteristics were used to optimize bacteria transport, retention, and release mechanisms. The Two Kinetics Sites model (Eq. (3)) was applied using HYDRUS-1D to model the process [6,23].

$$\frac{\partial \theta_m C_m}{\partial t} + \rho_b \frac{\partial S_1}{\partial t} + \rho_b \frac{\partial S_2}{\partial t} = \frac{\partial}{\partial x}\left(\theta_m D_m \frac{\partial C}{\partial x}\right) - \frac{\partial q C_m}{\partial x} \tag{3}$$

Where C is the bacteria concentration in the aqueous phase, (N_c: number of colloids), [$N_c\ L^{-3}$], S is the concentration of attached bacteria [$N_c\ M^{-1}$], ρ_b is the bulk density of the porous media [$M\ L^{-3}$], x is the distance in the vertical direction [L], and t is the time [T]. Subscripts 1 and 2 refer to the two different kinetics sites, respectively; other variables were defined earlier. The mass transfer between soil solution and both S_1 and S_2 sites [3,21] is:

$$\rho_b \frac{\partial S}{\partial t} = \rho_b \frac{\partial (S_1 + S_2)}{\partial t} = \theta \psi_t k_{att} C - \rho_b k_{\mathrm{det}} S_1 + \theta \psi_x k_{str} C \tag{4}$$

k_{att} and k_{det} are the attachment and detachment rate coefficients, respectively [T^{-1}], Ψ_t, and Ψ_x are time- or depth-dependent parameters describing deposition of bacteria due to retention by the solid phases. Adamczyk [24] suggested Langmuirian dynamics (Eq. (5)) for Ψ_t to explain blocking phenomena and Bradford et al. [25] proposed a depth-dependent blocking coefficient for straining process (Ψ_x), thus a simple and flexible function to account for time and depth-dependent bacteria deposition behavior (Eqs. (6) and (7), respectively).

$$\psi_t = 1 - \frac{S}{S_{\max}} \tag{5}$$

$$\psi_x = \left(\frac{d_c + z}{d_c}\right)^{-\beta} \tag{6}$$

$$\psi_s = \left(1 - \frac{S}{S_{\max}}\right)\left(\frac{d_c + z}{d_c}\right)^{-\beta} \tag{7}$$

In these equations, S is the solid phase concentration [$N_c\ M^{-1}$], S_{max} is the maximum solid phase concentration [$N_c\ M^{-1}$] of colloids on sorption sites, d_c is the mean diameter of sand particles [L], z is the coordination location where the straining process begins (the surface of sand columns in this study), and β was fixed at 0.43, as an empirical factor controlling the shape of the spatial distribution [-], suggested by Bradford et al. [25].

The retention process was assumed to be reversible. Therefore, for either the pulse, attachment (k_{att}), straining (k_{str}), or detachment (k_{det}), and release (k_{rele}), coefficients were predicted from the two sites (Eq. (4)). By extension, k_{det} and k_{att} were shown to be physico-chemical, and k_{str} and k_{rele} to be physical mechanisms [4,23].

For a bacterium that protrudes a distance, d_f, out of the film or out of the air-water-solid interface, the capillary potential energy, Φc (J), can be determined by integrating the capillary force in the direction of the water film development (Eqs. (8), (9)) [14,26,27].

$$F_{v-tot} = \sigma_{aw}\pi\sqrt{r_p{}^2 - \left(h_f - r_p\right)^2}\cos\left[\beta + \frac{\pi}{2} - \cos^{-1}\left(\frac{h_f - r_p}{r_p}\right)\right] \tag{8}$$

$$\Phi_c = \int_{z=rp(1-\cos\beta)}^{z=d_f} F_{v-tot}\,dz \tag{9}$$

$$= \int_{z=rp(1-\cos\beta)}^{z=d_f} \sigma_{aw}\pi\sqrt{r_p{}^2 - \left(h_f - r_p\right)^2}\cos\left[\beta + \frac{\pi}{2} - \cos^{-1}\left(\frac{h_f - r_p}{r_p}\right)\right]dz$$

Where σ_{aw} is the surface tension of the air-water interface (0.0718 N/m at 25 °C), β is the contact angle between water and bacteria (°), and z is the coordinate that passes through the center of the bacterium and is orthogonal to the water film.

2.5. Hydrophobic potential energy

Hydrophobic interaction energy between sand particles and air-water interfaces was estimated according to [28] (Eq. (10)).

$$\Phi^{hydr} = \int \frac{K_{123} r_p}{h^2} = -\frac{K_{123} r_p}{h} \tag{10}$$

Where K_{123} is a constant and r_p is the sand particle radius. For the asymmetric interactions between materials 1 and 2 in the medium 3, K_{123} can be estimated by following empirical relationship (Eq. (11)).

$$log K_{123} = a\left(\frac{\theta_1 + \theta_2}{2}\right) + b \tag{11}$$

Where θ_1 and θ_2 are the water contact angles (CAs) for the air-water interfaces (CA: 180°) [28] and for the water-sand interfaces; a and b are system-specific constants. For the interface interactions, values of a = − 5 and b = − 20 were used in this study according to Yoon et al. [28].

2.6. Hydrodynamic and resisting torques

Bacteria attached and/or trapped in the columns may be detached or released due to the hydrodynamic forces from water. A balance between the adhesive and the hydrodynamic forces can provide physico-chemical attachment under unfavorable conditions [27]. If the resisting torque ($T_{resisting}$) acting on bacteria at the grain surface is greater than the hydrodynamic torque ($T_{hydrodynamic}$), bacteria attachment on the surface of sand grain surface may take place [27]. Bradford et al. [29,30] used F_{DLVO} forces (N) to describe $T_{resisting}$ and $T_{hydrodynamic}$ for colloids attached in the secondary minimum as given in Eqs. (12) and (13), respectively.

$$T_{resisting} = \left(\frac{4 r_b F_{DLVO}}{K_i}\right)^{1/3} F_{DLVO} \tag{12}$$

Where r_b is the bacteria radius (m) and K_i is the elastic interaction constant (N/m^2). We used $K_i = 4.014 \times 10^9$ N/m^2, estimated for glass beads and colloids by Bergendahl [31]. The value of F_{DLVO} was calculated as Φ_{min2}/h_0 (based on DLVO theory data from Sepehrnia [12]; where Φ_{min2} is the secondary minimum interaction energy value (J) and h_0 is the separation distance between the bacteria and the grain surface (m) [31–33]. The pore-space morphology was simplified by considering it as capillary tubes of different sizes (ranging in radius from 2.5 to 100 μm), like other studies [19,27]. The hydrodynamic torque acting on the bacteria near to the solid interface due to the hydrodynamic shear force can be estimated using Eq. (13) [29,30].

$$T_{hydrodynamic} = 14.287\pi\mu_w r_p{}^3\frac{\partial v}{\partial r} = 7.1435\pi\mu_w r_p{}^3\frac{\Delta P}{L_{ct}}\left(R_{ct} - r_p\right) \tag{13}$$

Where μ_w is the water viscosity (Pa s), r_b is the bacteria radius (m), r is the radial direction from the solid surface (m), v is the pore scale velocity vector (m/s), $\partial v/\partial r$ is the velocity shear rate that acts on attached bacteria (1/s), R_{ct} is the radius of a capillary tube (m) and $\Delta P/L_{ct}$ is the gradient in pressure over the capillary tube length (N/m^3). In a porous medium (a given conductivity and Darcy velocity), $\Delta P/L_{ct}$ can be determined using Darcy's Law for horizontal flow [27].

3. Results and discussion

3.1. Bromide transport

Hydraulic properties of the wettable and water-repellent sand columns for dry infiltration (Pulse I) and wet infiltration (Pulse II) are presented in Table 1. The data for wettable sand columns were effectively captured by the model ($R^2 = 0.98–0.99$) with the highest standard error for the estimation of α in both pulses of the sand columns (Table S1). The K_s values were similarly estimated (1.20 and 1.57 cm min^{-1}), but the data were slightly less than the experimental value (3.8 cm min^{-1}) reported by Sepehrnia et al. [12] using the uniform model. The λ and α values of Br^- were higher from the first pulse to the second (Table 1) indicating the effect of the initial dry condition and the tendency for the exchange of solute mass with dry pore networks in wettable porous media. For the water-repellent sand ($R^2 = 0.66–0.99$) however, the K_s values of the two pulses were closely estimated with lower values than the lab data of the wettable sand (i.e., 1.1 cm min^{-1}, [12]). The peak values of λ (0.912 ± 0.28 cm^{-1}) and α (1.65 ± 1.55 cm^{-1}) occurred in the dry infiltration (Pulse I) of the wettable and water-repellent sand, respectively. The immobile water content was greater in the wet infiltration (Pulse II), with no difference between wettable and water-repellent sand, suggesting reduction or elimination of water repellency.

Overall, the separate modeling for either pulse by MIM was consistent with the uniform model performed by Sepehrnia et al. [12] that considered simultaneous simulation of the two pulses, but with a better resolution of solute exchange and dispersivity between the wettable and water-repellent sand in transition states. Fig. 1.

3.2. Bacteria fate

The experimental and simulated break through curves (BTCs) of bacteria are in Fig. 2a–d. The experimental data fitted well with the model ($R^2 = 0.78–0.96$) (Tables 2 and 3), however the model accuracy was decreased for the water-repellent sand medium (Tables S2 and S3).

In the dry infiltration pulse for the wettable sand, the value of S_{max} (linked to maximum solid phase concentration of deposited bacteria) was greater for *R. erythropolis* (1.37 ± 1.83) than *E. coli* (0.053 ± 0.02), but *R. erythropolis* also had a larger detachment rate (k_{det}:1.83 min^{-1}) than *E. coli* (k_{det}: 0.033 min^{-1}) (Table 2). The higher values of the k_{str} and k_{rele} rates for *R. erythropolis* (Table 2) compared to *E. coli* (0.0003 min^{-1}, Table 2), indicate a greater rate of physical retention. The 100-fold higher values of the k_{att} and k_{det} (0.033 min^{-1}) compared to the k_{str} and k_{rele} rates (0.0003 and 0.002 min^{-1}) illustrate the dominance of physiochemical mechanisms for *E. coli* [19]. The values of retention and release coefficients corresponded with Bai et al. [20] who explored *Klebsiella* sp. and *R. rhodochrous* transport in fine (0.36 mm diameter and porosity 0.34 ± 0.01) and coarse (0.90 mm diameter and porosity 0.45 ± 0.01) sand columns in unsaturated flow condition.

In the wet infiltration pulse, the values of S_{max} for both bacteria (*E. coli*: 0.07 ± 0.001, *R. erythropolis*: 0.03 ± 0.01) decreased. This, compared to the first pulse (*E. coli* 0.053 ± 0.02, *R. erythropolis* 1.37 ± 1.83), demonstrated that initial dry conditions of porous media play an important role in enhancing bacteria retention and an increase in transition water can remobilize the retained/attached bacteria [6,32]. Given that the immobile solid phase (e.g., soil) could be much more important than the air phase in determining colloid retention in unfavorable conditions of unsaturated porous media [7,34]. Additionally, Sepehrnia et al. [12] reported that hydrophobic potential energy for *E. coli* and *R. erythropolis* attachment to the air-water interfaces only becomes important at distances less than 0.2 and 2.2 nm, respectively. Bai et al. [21] found no relationship between S_{max} values and sand grain size in unsaturated flow condition for *Klebsiella* sp. and *R. rhodochrous*. Kasel et al. [35] reported that S_{max} values decreased with increasing grain size in saturated flow condition.

The data thus illustrated a greater rate of physical straining (k_{str} 14.73 and k_{rele} 9.98 min^{-1}) to physiochemical attachment (k_{att} 0.61 min^{-1} and k_{det} 9.73 min^{-1}) for hydrophilic *E. coli*, while hydrophobic *R. erythropolis* (with the smaller size) was very likely retained as a result of physiochemical mechanisms (k_{att} 14.23 min^{-1} and k_{det} 31.69 min^{-1}) in the wetted-state condition. These results demonstrate bacteria size and hydrophobicity effects for *E. coli* (2.05 μm), and *R. erythropolis* (1.47 μm), such that a bigger in size may be trapped in pores or clog the narrow pore spaces by the detachment from the grain surfaces [35], while hydrophobicity promotes attachment to retention sites [35]. This was also in agreement with mass balance data for those bacteria reported by Sepehrnia et al. [11,12].

Overall, the results demonstrated that hydrophobic *R. erythropolis* had greater affinity to get close to the grain surfaces of wettable sand particles in dry conditions. Due to the higher retention sites in the first pulse than the second pulse of the wettable sand (i.e., the higher S_{max} values) the bacteria could overcome repulsive forces and attach to the surfaces, likely causing straining by water films at very early time of infiltration (see k_{str} and k_{rele} values, Table 2). The latter can be ascertained from the higher values of the coefficients for *R. erythropolis* if compared with *E. coli* (Table 2) and the mass recovery reported by Sepehrnia et al. [12]. After leaching, the importance of straining decreased for *R. erythropolis* due to the increase of the water film thicknesses in the second pulse. However, hydrophilic *E. coli*, with a slightly greater size, had more complex behavior; on one hand, very similar coefficient values for k_{att} and k_{det} (Table 2) showed overcoming hydrophilic-hydrophilic repulsive forces (i.e., between bacteria and wettable sand particles [12,35–37]) and approaching particle surfaces due to the initial dry conditions. On the other hand, small values of physical retention may indicate bacteria detached because they experienced higher hydrodynamic stresses [29,36,37].

For the water-repellent sand, the S_{max} values for the dry infiltration pulse were greater than the wet infiltration pulse, and those values for *E. coli* were higher than *R. erythropolis*. In the wet infiltration pulse the S_{max} values were similar for both bacteria. This potentially indicates a greater probability of *E. coli* retention (Fig. 2c). The values of k_{str} coefficients were higher than k_{att} for both pulses (except for *E. coli* in the second pulse), suggesting greater physical retention of bacteria in the water-repellent sand compared to the wettable counterpart. By extension, in dry infiltration, *E. coli* had higher values of the k_{str} and k_{rele} rates (1.20 and 0.01 min^{-1}) compared to the k_{att} and k_{det} rates (0.30 and 0.0004 min^{-1}). *R. erythropolis* had a similar trend, but the differences were less (Table 3).

In the wet infiltration pulse, the data for *R. erythropolis* was unchanged even with a higher k_{str} and k_{rele} values than the earlier dry infiltration pulse (Table 3), and *E. coli* showed a noticeable higher value

Table 1
Hydraulic properties of the wettable and water-repellent sand columns for dry (Pulse I) and wet infiltration (Pulse II). K_s: inversed saturated water content, λ: dispersivity, θ_{im}: immobile water content, α: mass transfer coefficient for Br exchanged between mobile and immobile liquid regions. The data are the average of the columns treated with *E. coli* and *R. erythropolis*. R^2 donates the correlation between the observed Br^- break through curves and the fitted ones.

	K_s (cm min^{-1})	λ (cm^{-1})	θ_{im} (cm^3 cm^{-3})	α (cm^{-1})	R^2
Wettable sand					
Pulse I	1.54 (± 0.03)	0.126 (± 0.01)	0.002 (± 0.001)	1.61 (± 1.55)	0.99
Pulse II	1.20 (± 0.09)	0.095 (± 0.03)	0.014 (± 0.02)	0.09 (± 0.07)	0.98
Water repellent sand					
Pulse I	0.43 (± 0.05)	0.912 (± 0.28)	0.001 (± 0.001)	0.029 (± 0.03)	0.98
Pulse II	0.37 (± 0.01)	0.08 (± 0.04)	0.01 (± 0.02)	0.12 (± 0.08)	0.66

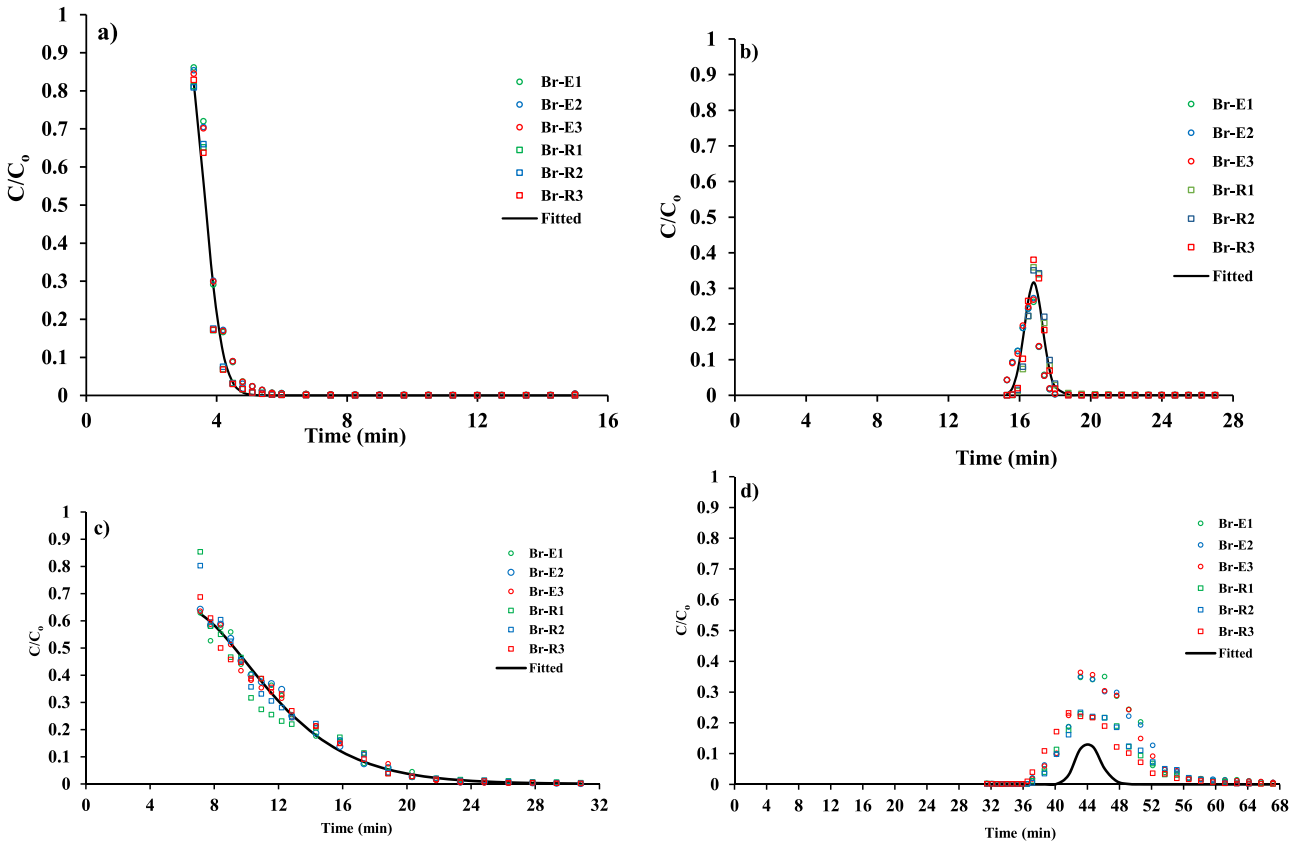

Fig. 1. Bromide breakthrough curves through wettable (a and b) and water-repellent (c and d) sand columns. E1–E3, and R1–R3 refer to replicates for *E. coli* and *R. erythropolis*, respectively.

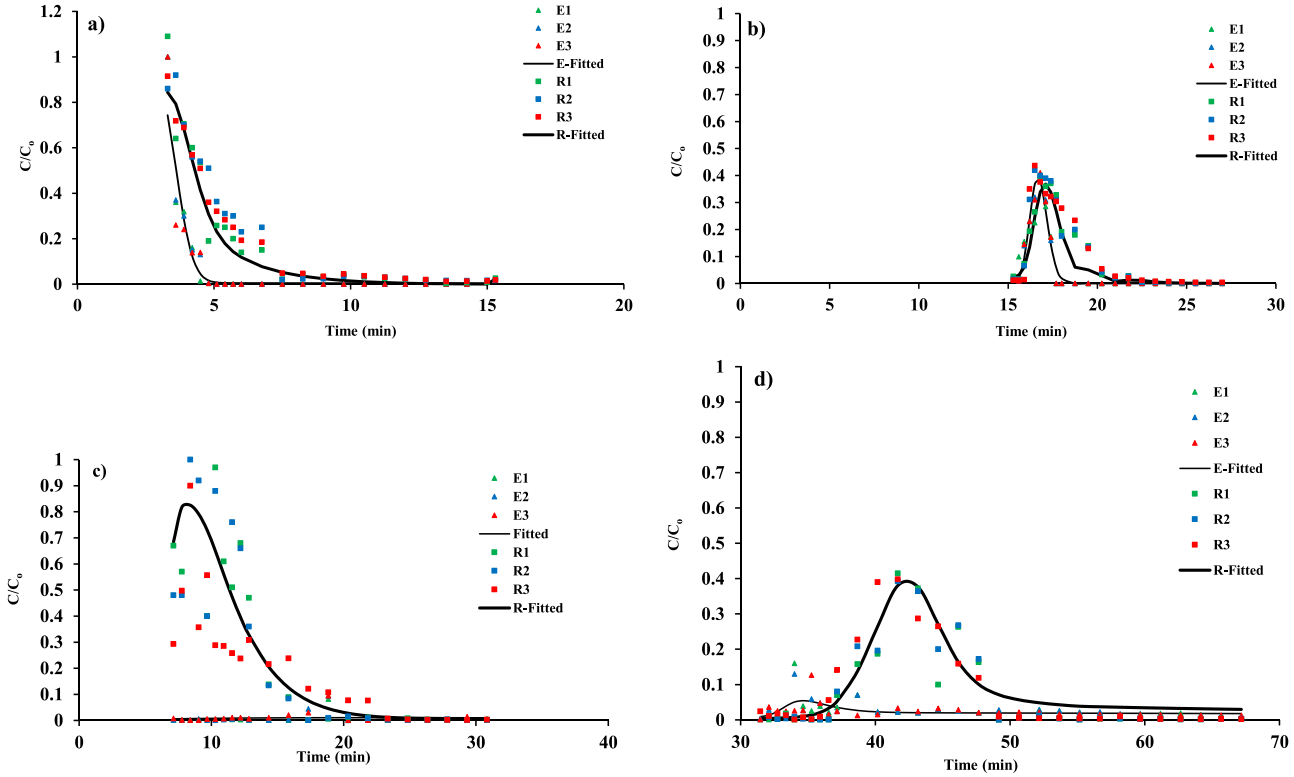

Fig. 2. *E. coli* (E1–E3) and *R. erythropolis* (R1–R3) breakthrough curves through wettable (a and b) and water-repellent (c and d) sand columns. The digits illustrate replicates.

Table 2
Transport, retention and release parameters (maximum solid phase concentration of deposited bacteria S_{max}, attachment coefficient k_{att}, detachment coefficient k_{det}, straining coefficient k_{str}, physical release coefficient k_{rele}) fitted using the effluent and the deposition concentrations of *E. coli* and *R. erythropolis* for the wettable sand. R^2 donates the correlation between the observed bacteria break through curves and the fitted ones.

	Bacteria/parameter	S_{max}	k_{att}	k_{det}	k_{str}	k_{rele}	R^2
Pulse I	*E. coli*	0.053 (± 0.02)	0.033 (± 0.001)	0.033 (± 0.003)	0.0003 (± 0.0001)	0.002 (± 0.002)	0.91 (± 0.04)
	R. erythropolis	1.37 (± 1.83)	0.37 (± 0.08)	1.83 (± 0.47)	4.15 (± 0.89)	3.69 (± 0.76)	0.96 (± 0.04)
Pulse II	*E. coli*	0.07 (± 0.001)	0.61 (± 0.41)	9.73 (± 0.46)	14.73 (± 4.32)	9.98 (± 0.40)	0.94 (± 0.01)
	R. erythropolis	0.03 (± 0.01)	14.23 (± 1.52)	31.69 (± 6.60)	2.82 (± 0. 34)	1.41 (± 0.16)	0.96 (± 0.02)

Table 3
Transport, retention and release parameters (maximum solid phase concentration of deposited bacteria S_{max}, attachment coefficient k_{att}, detachment coefficient k_{det}, straining coefficient k_{str}, physical release coefficient k_{rele}) fitted using the effluent and the deposition concentrations of *E. coli* and *R. erythropolis* for the water-repellent sand. R^2 donates the correlation between the observed bacteria break through curves and the fitted ones.

	Bacteria/parameter	S_{max}	k_{att}	k_{det}	k_{str}	k_{rele}	R^2
Pulse I	*E. coli*	1.10 (± 0.043)	0.30 (± 0.005)	0.0004 (± 0.002)	1.20 (± 0.013)	0.01 (± 0.0002)	0.78 (± 0.03)
	R. erythropolis	0.14 (± 0.25)	0.00003 (± 0.00002)	0.032 (± 0.03)	0.27 (± 0.45)	0.06 (± 0.06)	0.78 (± 0.08)
Pulse II	*E. coli*	0.01 (± 0.002)	0.62 (± 0.164)	0.64 (± 1.10)	0.37 (± 0.04)	1.51 (± 1.57)	0.80 (± 0.06)
	R. erythropolis	0.03 (± 0.002)	5.45 (± 5.00)	0.14 (± 0.11)	24.00 (± 1.73)	5.91 (± 0.19)	0.94 (± 0.050)

for the k_{rele} (1.51 min^{-1}) but equal values for k_{att} and k_{det} rates (0.62 and 0.64 min^{-1}). The difficulties in characterizing a robust mechanism for *E. coli* (also see dry infiltration Pulse I, wettable sand, Table 2), may indicate a combination of mechanisms affect retention processes due to the larger size and the initial dry condition of the columns. The data illustrate that water film thicknesses increased very slowly in the water-repellent sand columns and bacteria were highly retained in films smaller than the bacteria diameter for a longer time (particularly in the first pulse if compared with the wettable sand). The faster physical release rate (k_{rele}: 5.91 min^{-1}) for *R. erythropolis* compared to *E. coli* (1.5 min^{-1}) again illustrates bacteria size and thus demonstrates that *E. coli* retention in the water films for longer times could increase the probability of higher attachment to the particles (k_{att}: 0.62 min^{-1}). The latter was also supported by mass recovery information where only 15 % of *E. coli* were recovered vs. 92 % for *R. erythropolis* [8]. Therefore *E. coli* experienced greater physical retention in the form of film straining than physicochemical straining. The detachment coefficients also suggest that *E. coli* experienced hydrodynamic stresses due to their larger size [29,37], as described below. Such complex behavior of *E. coli* may also indicate that in addition to hydrophobicity/hydrophilicity, bacteria strains have various cell properties (e.g., flagella) that simultaneously influence their fate [38]. Therefore, to reach global conclusions, future studies should focus on various mutants of the same strain. For example, Zheng et al. [38] reported that flagellar modifications affect *Salmonella enterica serovar Typhimurium* transport and retention in different ways in environmental conditions. One very promising technique is also benefiting from DNA-based tracers recently studied by scholars [39,40].

Table 4
The hydrodynamic ($T_{hydrodynamic}$) and resisting ($T_{resisting}$) torques calculated for *E. coli* and *R. erythropolis* in several different sized capillary tubes for wettable and water-repellent sands.

	Wettable sand			Water-repellent sand	
	E. coli	*R. erythropolis*		*E. coli*	*R. erythropolis*
Pore size (μm)	$T_{hydrodynamic}$ (NM)	$T_{hydrodynamic}$ (NM)	Pore size (μm)	$T_{hydrodynamic}$ (NM)	$T_{hydrodynamic}$ (NM)
0.1	-1.5×10^{-16}	-1.5×10^{-16}	0.005	-2.58×10^{-16}	-1×10^{-16}
0.15	-1.4×10^{-16}	-1.4×10^{-16}	0.01	-2.6×10^{-16}	-1×10^{-16}
0.3	-1.2×10^{-16}	-1.2×10^{-16}	0.014	-2.6×10^{-16}	-1×10^{-16}
0.75	-4.3×10^{-17}	-4.3×10^{-17}	0.035	-2.5×10^{-16}	-1×10^{-16}
1.5	8.28×10^{-17}	8.28×10^{-17}	0.07	-2.4×10^{-16}	-9.8×10^{-17}
3	3.34×10^{-16}	3.34×10^{-16}	0.14	-2.2×10^{-16}	-9×10^{-17}
5	6.69×10^{-16}	2.71×10^{-16}	0.23	-2×10^{-16}	-8×10^{-17}
15	2.34×10^{-15}	9.5×10^{-16}	0.702	-7.7×10^{-17}	-3.1×10^{-17}
30	4.86×10^{-15}	1.97×10^{-15}	1.41	1.05×10^{-16}	4.25×10^{-17}
75	1.24×10^{-14}	5.02×10^{-15}	3.51	6.5×10^{-16}	2.63×10^{-16}
149	2.5×10^{-14}	1.01×10^{-14}	7.02	1.56×10^{-15}	6.32×10^{-16}
299	5.01×10^{-14}	2.03×10^{-14}	14.1	3.38×10^{-15}	1.37×10^{-15}
14,912	2.51×10^{-12}	1.02×10^{-12}	703	1.82×10^{-13}	7.36×10^{-14}
	Wettable sand	Water-repellent sand			
	$T_{rsisting}$ (NM)				
E. coli	1.99×10^{-19}			5.34×10^{-22}	
R. erythropolis	1.79×10^{-19}			1.91×10^{-23}	

3.3. Impacts of hydrodynamic and resisting torques

Both bacteria experienced higher hydrodynamic torques in the wettable sand columns compared to the water repellent sand (Table 4). Negative hydrodynamic torques showed a broader range of pores in the water-repellent sand compared to the wettable sand (Table 4). The negative torques conceptually mean bacteria rotating clockwise in the pores; however, the negative values occurred when pore radius was smaller than the bacteria radius. This might indirectly illustrate that either some pores were not big enough to pass bacteria, or bacteria were transported due to their smaller dimensions.

To test this further, we compared bacteria and pore sizes. Both the widths (*E. coli*: 1.2 μm, *R. erythropolis*: 1.1 μm) and lengths (*E. coli*; 2.05 μm, *R. erythropolis*: 1.47 μm, [128]) of the bacteria were larger than the pore sizes where the hydrodynamic torques were negative (Table 4). The negative values thus show the inactive torques in the pores, rather than the bacteria dimension impacts. In negative torque ranges, one of the interesting results was a greater contribution of the water-repellent sand pores compared to wettable sand pores. This is coincident with the nature of water repellency, because it can impede water flow (e.g., low *Ks* values, Table 1) through soil in unsaturated conditions. Therefore, those pores were probably inactive in bacterial transport. Such pore range sizes (2.5–100 μm) were also evaluated by [29] to calculate hydrodynamic and resisting torques.

The $T_{hydrodynamic}$ was greater than $T_{resisting}$ in all cases (Table 4). This showed that bacteria detachment is possible in both wettable and water repellent sand columns. In the wettable sand columns where the bacteria attachment conditions were unfavorable (high electrostatic repulsive forces; [28]), $T_{hydrodynamic}$ resulted in enhanced detachment and thus drainage (k_{det} in Table 2 vs. Table 3). $T_{hydrodynamic}$ acted more on *E. coli* compared to *R. erythropolis* in both systems (Table 4), however, $T_{hydrodynamic}$ could also cause increased bacteria retention (Fig. 2a–b vs. Fig. 2c–d) by forcing bacteria into regions where water velocity was slow, and probably water-air interfaces were still present [6,9]. The latter may be more possible for *E. coli* in the water-repellent sand columns, because they may remain unsaturated for a longer time compared to the wettable counterpart due to persistence of water repellency (Fig. 2d).

3.4. Capillary potential forces and water film thinning

Dry infiltration followed by imbibition and drainage cycles could confront bacteria with trapping in water films at very early times (imbibition) and at the later times (drainage) (graphical abstract). Therefore, one plausible retention mechanism for bacteria in our experimental conditions was capillary potential forces in which bacteria could be retained within the thin water films (Fig. 3). Capillary energy potential profiles of *E. coli* and *R. erythropolis* were thus calculated as a function of the distance protruded for both bacteria within the thin water film. This energy is highly dependent on protrusion distance [21]. For distances less than 395 nm, the capillary potential energy for *E. coli* was less than for *R. erythropolis* for the same distance of protrusion through the water films (Fig. 3a). However, this was reversed in tendency for distances greater than 395 nm, where hydrophilic *E. coli* had a higher capillary energy potential than hydrophobic *R. erythropolis*. Furthermore, evaluation of the energy profile showed that the water-repellent sand had considerable capillary potential energy for a longer distance (12.8 nm) in comparison to the wettable sand (0.16 nm) (Fig. 3b). The data correspond with previous studies [20], including similar results found for *Klebsiella* sp. and *R. rhodochrous* but for distances less than 500 nm [20].

The capillary potential energy profiles of bacteria and sand indicate favorable retention conditions for bacteria in water-repellent sand columns compared to wettable counterparts. Moreover, smaller, hydrophobic *R. erythropolis* were more readily trapped in water films, but also released at greater concentrations more rapidly. Larger hydrophilic

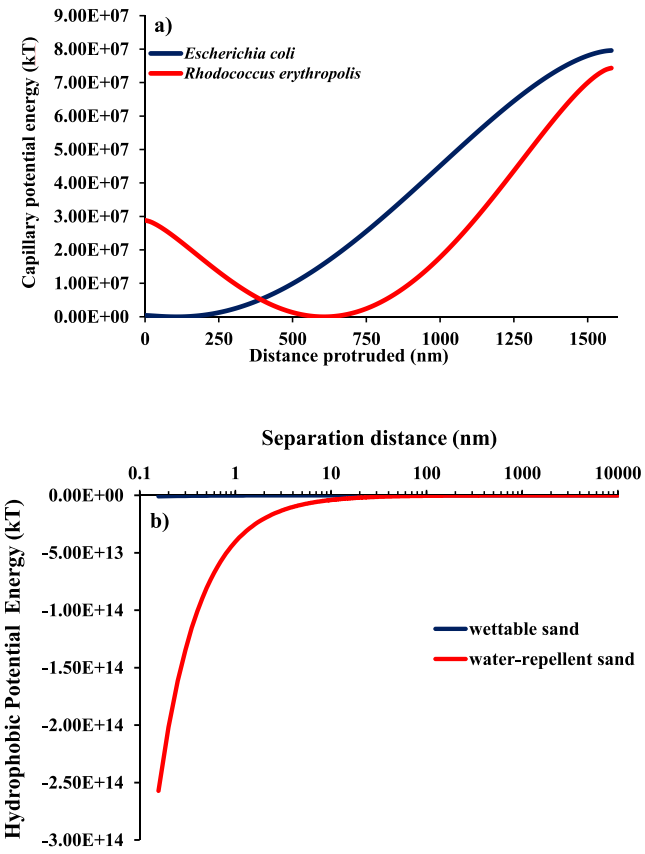

Fig. 3. Calculated capillary and hydrophobic potential energy profiles as a function of the distance protruded for *E. coli* and *R. erythropolis* retained within the thin water films (a) and for the wettable and water-repellent sand media (b).

E. coli, on the other hand, could be firmly retained for long distances and times. The distances (> 400 nm for *E. coli* and > 600 nm for *R. erythropolis*) may describe the higher retention of *E. coli* and proportionally greater release of *R. erythropolis* in the experiments (Fig. 2c–d). Colloids attach to the collector surfaces mobilized by the strong capillary forces induced by the moving gas-water interface and transport along with the interface [34]. However, hydrophilic colloids compared to the hydrophobic ones redeposit on gas-water-solid interfaces or thin water films because of their greater capillary potential [34,36]. Pan et al. [40, 41] found the short-range hydrophobic force is responsible for rupturing wetting films formed on a hydrophobic surface (CA: 81°), while the long-range hydrophobic force is responsible for accelerated film thinning that coincides with *R. erythropolis* release and *E. coli* retention in our experiments, respectively. The results demonstrate considerable retention of *E. coli* observed in the water-repellent columns (Fig. 2c–d vs. 2a–b), which was also supported by HYDRUS simulations discussed earlier.

4. Conclusion

A leaching experiment and inverse modeling were undertaken to illustrate the dominant retention mechanisms of hydrophilic *E. coli* and hydrophobic *R. erythropolis* under contrasting hydraulic and wettability conditions. To better isolate the effects of straining and attachment, analysis of torques and capillary potential energy for film straining were performed. The results robustly illustrated the effects of porous media wettability, and the contrasting water conditions (air-dried and respective wetted-state infiltration) on Br^- transport. A smaller hydraulic conductivity, a greater Br^- dispersivity, and a smaller rate of mass transfer between mobile and immobile zones were found in Br^-

data in dry infiltration of water into the water-repellent sand compared to a wettable sand counterpart.

The dominant bacteria retention process was distinct between a first dry infiltration pulse and subsequent wet infiltration pulse in the wettable sand. The data illustrated attachment for *E. coli* and straining for *R. erythropolis* in dry infiltration; however, the exact opposite mechanism was found for the strains in subsequent wet infiltration. The main mechanism of water-repellent sand for bacteria retention was straining, with a considerable mass retention for *E. coli* compared to *R. erythropolis*. Hydrodynamic torque acted on and detached bacteria; however, water-repellency provided favorable interfaces with interaction capillary energies to retain *E. coli* and *R. erythropolis* in the form of film straining at very early stages of imbibition and at later periods of drainage.

CRediT authorship contribution statement

Nasrollah Sepehrnia: Conceptualization, Data curation, Formal analysis, Funding acquisition, Investigation, Methodology, Project administration, Resources, Software, Supervision, Validation, Visualization, Writing – original draft, Writing – review & editing. **Mohsen Gorakifard:** Data curation, Investigation, Methodology, Software, Writing – review & editing. **Paul D. Hallett:** Funding acquisition, Resources, Supervision, Validation, Writing – review & editing. **Mohammad Ali Hajabbasi:** Resources, Validation, Visualization, Writing – review & editing. **Nima Shokri:** Validation, Visualization, Writing – review & editing. **Mark Coyne:** Validation, Visualization, Writing – review & editing.

Declaration of Competing Interest

The authors declare that they have no known competing financial interests or personal relationships that could have appeared to influence the work reported in this paper.

Data Availability

Data will be made available on request.

Acknowledgements

This project has received funding from the European Union's Horizon 2020 research and innovation programme under the Marie Skłodowska-Curie Grant agreement no. 101026287. We acknowledge University of Aberdeen, UK for supporting this project.

Appendix A. Supporting information

Supplementary data associated with this article can be found in the online version at doi:10.1016/j.colsurfb.2023.113433.

References

[1] N. Sepehrnia, L. Memarianfard, A.A. Moosavi, J. Bachmann, F. Rezanezhad, M. Sepehri, Retention modes of manure-fecal coliforms in soil under saturated hydraulic, J. Environ. Manag. 227 (2018) 209–215, https://doi.org/10.1016/j.jenvman.2018.08.086.

[2] N. Sepehrnia, A.A. Mahboubi, M.R. Mosaddeghi, A.S. Sinejani, G. Khodakaramian, Escherichia coli transport through intact gypsiferous and calcareous soils during saturated and unsaturated flows, Geoderma 217 (2014) 83–89.

[3] N. Sepehrnia, L. Memarianfard, A.A. Moosavi, J. Bachmann, G. Guggenberger, F. Rezanezhad, Bacterial mobilization and transport through manure enriched soils: experiment and modeling, J. Environ. Manag. 201 (2017) 388–396, https://doi.org/10.1016/j.jenvman.2017.07.009.

[4] N. Sepehrnia, S.H. Tabatabaei, H. Norouzi, M. Gorakifard, H. Shirani, F. Rezanezhad, Particle fractionation controls Escherichia coli release from solid manure, Heliyon 7 (2021), e07038, https://doi.org/10.1016/j.heliyon.2021.e07038.

[5] S.A. Bradford, S. Torkzaban, Colloid transport and retention in unsaturated porous media: a review of interface-, collector-, and pore-scale processes and models, Vadose Zo. J. 7 (2008) 667–681, https://doi.org/10.2136/vzj2007.0092.

[6] S.A. Bradford, V.L. Morales, W. Zhang, R.W. Harvey, A.I. Packman, A. Mohanram, C. Welty, Transport and fate of microbial pathogens in agricultural settings, Crit. Rev. Environ. Sci. Technol. 43 (2013) 775–893, https://doi.org/10.1080/10643389.2012.710449.

[7] S.A. Bradford, Y. Wang, S. Torkzaban, J. Šimůnek, Modeling the release of E. coli D21g with transients in water content, Water Resour. Res. 51 (2015) 3303–3316, https://doi.org/10.1002/2014WR016566.

[8] H.N. Kim, S.A. Bradford, S.L. Walker, *Escherichia coli O157: H7* transport in saturated porous media: role of solution chemistry and surface macromolecules, Environ. Sci. Technol. 43 (2009) 4340–4347, https://doi.org/10.1021/es8026055.

[9] C. Wang, R. Wang, Z. Huo, E. Xie, H.E. Dahlke, Colloid transport through soil and other porous media under transient flow conditions—a review, Wiley Interdiscip. Rev. Water 7 (2020), e1439, https://doi.org/10.1002/wat2.1439.

[10] J.T. Crist, Y. Zevi, J.F. McCarthy, J.A. Throop, T.S. Steenhuis, Transport and retention mechanisms of colloids in partially saturated porous media, Vadose Zo. J. 4 (2005) 184–195, https://doi.org/10.2136/vzj2005.0184.

[11] N. Sepehrnia, J. Bachmann, M.A. Hajabbasi, F. Rezanezhad, L. Lichner, P. D. Hallett, M. Coyne, Transport, retention, and release of *Escherichia coli* and *Rhodococcus erythropolis* through dry natural soils as affected by water repellency, Sci. Total Environ. 694 (2019), 133666, https://doi.org/10.1016/j.scitotenv.2019.133666.

[12] N. Sepehrnia, J. Bachmann, M.A. Hajabbasi, M. Afyuni, M. Horn, Modeling transport of *Escherichia coli* and *Rhodococcus erythropolis* through wettable and repellent porous media, Colloids Surf. B Biointerfaces 172 (2018) 280–287, https://doi.org/10.1016/j.colsurfb.2018.08.044.

[13] N. Sepehrnia, O. Fishkis, B. Huwe, J. Bachmann, Natural colloid mobilization and leaching in wettable and water repellent soil under saturated condition, Hydrol. Hydromech. 66 (3) (2018) 271–278, https://doi.org/10.1515/johh-2017-0058.

[14] J. Bachmann, S. Söffker, N. Sepehrnia, M.-O. Goebel, S.K. Woche, The effect of temperature and wetting–drying cycles on soil wettability: dynamic molecular restructuring processes at the solid–water–air interface, Eur. J. Soil Sci. 72 (5) (2021) 2180–2198, https://doi.org/10.1111/ejss.13102.

[15] S. Bakhshian, H.S. Rabbani, S.A. Hosseini, N. Shokri, New insights into complex interactions between heterogeneity and wettability influencing two-phase flow in porous media, Geophys. Res. Lett. 47 (2020), e2020GL088187, https://doi.org/10.1029/2020GL088187.

[16] H.S. Rabbani, V. Joekar-Niasar, N. Shokri, Effects of intermediate wettability on entry capillary pressure in angular pores, J. Colloid Interface Sci. 473 (2016) 34–43, https://doi.org/10.1016/j.jcis.2016.03.053.

[17] H.S. Rabbani, B. Zhao, R. Juanes, N. Shokri, Pore geometry control of apparent wetting in porous media, Sci. Rep. 8 (2018) 1–8, https://doi.org/10.1038/s41598-018-34146-8.

[18] N. Jarvis, A. Etana, F. Stagnitti, Water repellency, near-saturated infiltration and preferential solute transport in a macroporous clay soil, Geoderma 143 (2008) 223–230, https://doi.org/10.1016/j.geoderma.2007.11.015.

[19] J.T. Gannon, V.B. Manilal, M. Alexander, Relationships between cell surface properties and transport of bacteria through soil, Appl. Environ. Microbiol. 57 (1) (1991) 190–193, https://doi.org/10.1128/aem.57.1.190-193.1991.

[20] H. Bai, N. Cochet, A. Pauss, E. Lamy, Bacteria cell properties and grain size impact on bacteria transport and deposition in porous media, Colloids Surf. B Biointerfaces 139 (2016) 148–155, https://doi.org/10.1016/j.colsurfb.2015.12.016.

[21] H. Bai, N. Cochet, A. Pauss, E. Lamy, DLVO, hydrophobic, capillary and hydrodynamic forces acting on bacteria at solid-air-water interfaces: their relative impact on bacteria deposition mechanisms in unsaturated porous media, Colloids Surf. B Biointerfaces 150 (2017) 41–49, https://doi.org/10.1016/j.colsurfb.2016.11.004.

[22] C.H. Bolster, S.L. Walker, K.L. Cook, Comparison of Escherichia coli and Campylobacter jejuni transport in saturated porous media, J. Environ. Qual. 35 (2006) 1018–1025, https://doi.org/10.2134/jeq2005.0224.

[23] J. Šimůnek, M.T. van Genuchten, Modeling nonequilibrium flow and transport processes using HYDRUS, Vadose Zo. J. 7 (2008) 782–797, https://doi.org/10.2136/vzj2007.0074.

[24] Z. Adamczyk, T. Dabros, J. Czarnecki, T.G. Van De Ven, Particle transfer to solid surfaces, Adv. Colloid Interface Sci. 19 (1983) 183–252.

[25] S.A. Bradford, J. Simunek, M. Bettahar, M.T. Van Genuchten, S.R. Yates, Modeling colloid attachment, straining, and exclusion in saturated porous media, Environ. Sci. Technol. 37 (2003) 2242–2250.

[26] B. Gao, T.S. Steenhuis, Y. Zevi, V.L. Morales, J.L. Nieber, B.K. Richards, J. F. McCarthy, J.Y. Parlange, Capillary retention of colloids in unsaturated porous media, Water Resour. Res. 44 (2008), https://doi.org/10.1029/2006WR005332.

[27] V.I. Syngouna, C.V. Chrysikopoulos, Cotransport of clay colloids and viruses in water saturated porous media, Colloids Surf. A Physicochem. Eng. Asp. 416 (2013) 56–65, https://doi.org/10.1016/j.colsurfa.2012.10.018.

[28] R.H. Yoon, D.H. Flinn, Y.I. Rabinovich, Hydrophobic interactions between dissimilar surfaces, J. Colloid Interface Sci. 185 (1997) 363–370, https://doi.org/10.1006/jcis.1996.4583.

[29] S.A. Bradford, S. Torkzaban, S.L. Walker, Coupling of physical and chemical mechanisms of colloid straining in saturated porous media, Water Res. 41 (2007) 3012–3024, https://doi.org/10.1016/j.watres.2007.03.030.

[30] S.A. Bradford, H.N. Kim, B.Z. Haznedaroglu, S. Torkzaban, S.L. Walker, Coupled factors influencing concentration-dependent colloid transport and retention in saturated porous media, Environ. Sci. Technol. 43 (2009) 6996–7002, https://doi.org/10.1021/es900840d.

[31] J. Bergendahl, D. Grasso, Prediction of colloid detachment in a model porous media: hydrodynamics, Cem. Eng. Sci. 55 (2000) 1523–1532, https://doi.org/10.1016/S0009-2509(99)00422-4.
[32] B.V. Derjaguin, L.D. Landau, Theory of the stability of strongly charged lyophobic sols and of the adhesion of strongly charged particles in solutions of electrolytes, Acta Physicochim. USSR 14 (1941) 733–762, https://doi.org/10.1016/0079-6816(93)90013-L.
[33] E.J.W. Verwey, J.T.G. Overbeek, Theory of the Stability of Lyophobic Colloids, Elsevier, Amsterdam, 1948, https://doi.org/10.1021/j150453a001.
[34] S. Nishad, R.I. Al-Raoush, Colloid retention and mobilization mechanisms under different physicochemical conditions in porous media: a micromodel study, Powder Technol. 377 (2021) 163–173, https://doi.org/10.1016/j.powtec.2020.08.086.
[35] D. Kasel, S.A. Bradford, J. Šimůnek, M. Heggen, H. Vereecken, E. Klumpp, Transport and retention of multi-walled carbon nanotubes in saturated porous media: effects of input concentration and grain size, Water Res. 47 (2013) 933–944, https://doi.org/10.1016/j.watres.2012.11.019.
[36] P. Bhuvankar, A. Cihan, J. Birkholzer, Pore-scale CFD simulations of clay mobilization in natural porous media due to freshwater injection, Chem. Eng. Sci. 247 (2022), https://doi.org/10.1016/j.ces.2021.117046.
[37] H. Ma, C. Bolster, W.P. Johnson, K. Li, E. Pazmino, K.M. Camacho, S. Mitragotri, Coupled influences of particle shape, surface property and flow hydrodynamics on rod-shaped colloid transport in porous media, J. Colloid Interface Sci. 577 (2020) 471–480, https://doi.org/10.1016/j.jcis.2020.05.022.
[38] X. Zheng, H. Bai, Y. Tao, M. Achak, Y. Rossez, E. Lamy, Flagellar phenotypes impact on bacterial transport and deposition behavior in porous media: case of *Salmonella enterica Serovar Typhimurium*, Int. J. Mol. Sci. 23 (2022) 14460, https://doi.org/10.3390/ijms232214460.
[39] C. Wang, C.P. McNew, S.W. Lyon, M.T. Walter, T.H. Volkman, N. Abramson, H. E. Dahlke, Particle tracer transport in a sloping soil lysimeter under periodic, steady state conditions, J. Hydrol. 569 (2019) 61–76, https://doi.org/10.1016/j.jhydrol.2018.11.050.
[40] N. Sepehrnia, M. Yiyu, P.D. Hallett, Y. Tanino, C. Gubray-Rangin, Impacts of microplastics on bacteria transport and fate as evaluated using silica-DNA microparticles and bromide, ECIS, 2023, September 3rd–8th, Italy.
[41] L. Pan, S. Jung, R.H. Yoon, Effect of hydrophobicity on the stability of the wetting films of water formed on gold surfaces, J. Colloid Interface Sci. 361 (2011) 321–330, https://doi.org/10.1016/j.jcis.2011.05.057.